INORGANIC CHEMISTRY
FRONTIERS

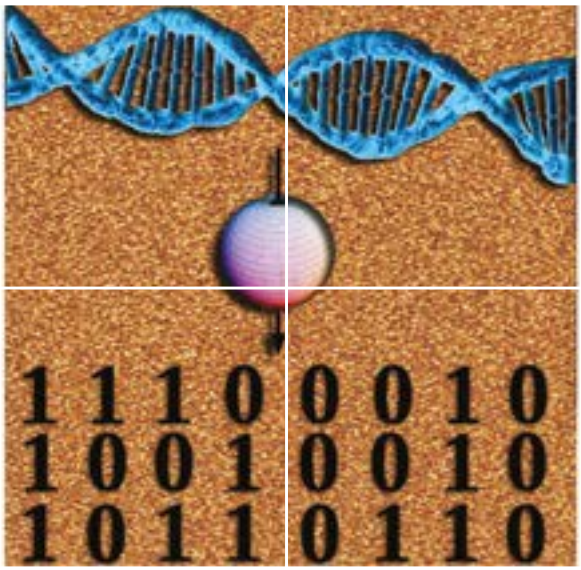

Accepted Manuscript

This article can be cited before page numbers have been issued, to do this please use: Y. Zheng, J. Han, L. Takele, F. Xie, Y. Zhang, J. Sun, B. Han, J. Chen, Y. Gao and Z. Tang, *Inorg. Chem. Front.*, 2019, DOI: 10.1039/C9QI00297A.

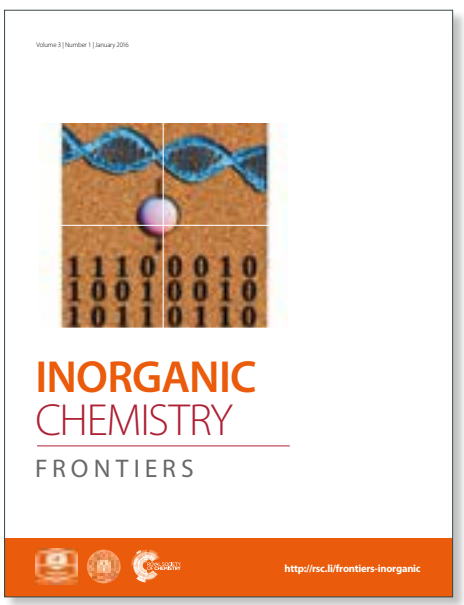

This is an Accepted Manuscript, which has been through the Royal Society of Chemistry peer review process and has been accepted for publication.

Accepted Manuscripts are published online shortly after acceptance, before technical editing, formatting and proof reading. Using this free service, authors can make their results available to the community, in citable form, before we publish the edited article. We will replace this Accepted Manuscript with the edited and formatted Advance Article as soon as it is available.

You can find more information about Accepted Manuscripts in the author guidelines.

Please note that technical editing may introduce minor changes to the text and/or graphics, which may alter content. The journal's standard Terms & Conditions and the ethical guidelines, outlined in our author and reviewer resource centre, still apply. In no event shall the Royal Society of Chemistry be held responsible for any errors or omissions in this Accepted Manuscript or any consequences arising from the use of any information it contains.

View Article Online
DOI: 10.1039/C9QI00297A

ARTICLE

Poly-phenylenediamine-derived Atomically Dispersed Ni Sites for Electroreduction of CO_2 to CO

Received 00th January 20xx,
Accepted 00th January 20xx

DOI: 10.1039/x0xx00000x

Yonglong Zheng, [a,b] Jianyu Han, [a] Leta Takele, [a,b] Feng Xie, [a,c] Yin Zhang, [a,b] Jiqing Sun, [a,b] Bing Han, [a] Jing Chen, [a] Yan Gao, *[a,b] and Zhiyong Tang [a,b]

CO_2 electroreduction is a promising technique for the management of the global carbon balance by low-grade renewable electricity. However, the lack of high efficient and selective catalyst has frustrated the development of this area. Here, we report a poly-phenylenediamine-derived atomically dispersed Ni catalyst as a highly efficient and selective electrocatalyst for the conversion of CO_2 to CO. The catalyst exhibited efficient production of CO with high Faradaic efficiency (FE) (90%) and a large current density of 11.6 mA cm^{-2} at −0.8 V *vs.* reversible hydrogen electrode (RHE). An excellent turnover frequency (TOF) of 3079 h^{-1} for electroreduction of CO_2 was also achieved at −0.8 V *vs.* RHE.

1. Introduction

Converting CO_2 into valuable chemicals via electroreduction process under mild conditions is a promising approach to reduce the emission of the greenhouse CO_2 into atmosphere. To facilitate the CO_2 electroreduction process, the development of high-selective catalysts with low overpotential and large TOF is highly desirable. However, traditional metallic catalysts such as Au, Ag, Cu and Sn usually suffer from high cost, large overpotentials and poor stability, which greatly hinder their practical applications. [1-4] Therefore, the development of highly efficient and low-cost electrocatalysts for the reduction of CO_2 is of paramount importance for both fundamental studies and practical applications. [5, 6]

Recently, researchers have developed different strategies for the synthesis of high-performance catalysts, especially in the new hot spot of single-atom catalysts (SACs). [7-11]

The SACs are a new kind of catalyst reaching the lowest size limit to obtain the maximum atom efficiency and expose the most active sites in catalysts.[12] The SACs combine the advantages from both heterogeneous catalysts and homogeneous catalyst. High atom utilization, improved stability and excellent recyclability are realized simultaneously.[13] Because of the great potentiality in improving the catalytic activity, the SACs have drawn lots of attention in thermocatalytic reaction, photocatalytic reaction and electrocatalytic reaction.[14] The catalytic efficiency was greatly improved by employing SACs in important reactions such as CO oxidation[15], methane conversion[16] , N_2 reduction[17], H_2 evolution[18, 19] and oxygen reduction reactions (ORR).[8,14,20] Since similar reaction path was found between ORR and CO_2 reduction reactions, further utilization of SACs in the area of electrochemical CO_2 reduction is highly expected. [21, 22] Several pioneering works have been done by different groups. Various transitional single-atom catalysts such as single Fe, Co, Ni, Cu, Zn sites were reported as high active catalysts for CO_2 reduction. [23-28] Among the various transitional single-atom catalysts, single Ni sites drew much more attention. Unlike other transitional single-atom catalyst, the single Ni sites can be prepared from a variety of precursors including polymer, Metal-organic frameworks (MOFs), graphene, and amino acid. [29-32] The chemical configuration and unsaturated sites of single Ni sites were intensively investigated to give a clear view on the critical role of Ni atoms in catalyzing CO_2-to-CO conversion. [33, 34] Remarkable activity and selectivity were achieved towards CO_2 reduction for the SACs of Ni. Despite the high activity manifested by the reported SACs of Ni, the synthesizing procedures are usually involved with sophisticated instruments and expensive reagents. Thus, a facile and universal synthesizing method is highly required. Here, in this work, we introduce a simple and low-cost method to prepare a carbon supported atomically dispersed Ni catalyst as an efficient electrocatalyst for CO_2 reduction. The catalyst was prepared by hard template synthesis and carbonization at high temperature. Atomically dispersed Ni was introduced via the simple addition of $NiCl_2$ at the first beginning which means the introducing of single atom is a facile and universal method. The subtract supporting the single atom was made from a commonly used polymer which is economically feasible. Hierarchically porous structure was achieved with the help of SiO_2 template. These advantages make our SACs have great

[a] CAS Key Laboratory of Nanosystem and Hierarchical Fabrication, CAS Center for Excellence in Nanoscience, National Center for Nanoscience and Technology, Beijing 100190, China. Corresponding author. E-mail: gaoyan@nanoctr.cn
[b] University of Chinese Academy of Sciences, Beijing 100049, China.
[c] Advanced Membranes and Porous Materials Center, Physical Science and Engineering Division, King Abdullah University of Science and Technology, Thuwal 23955-6900, Saudi Arabia

Electronic Supplementary Information (ESI) available: See DOI: 10.1039/x0xx00000x

potential for the mass production in the practical application. The prepared single-atom catalyst (denoted as Ni-C-N) showed a maximum FE of 90% toward CO formation and an excellent TOF of 3079 h^{-1} at −0.8 V *vs.* RHE.

2. Experimental section

Chemicals and materials M-Phenylenediamine (MPD, 99%), colloidal silica (LUDOX(R) HS-40 colloidal silica 40 wt. % suspension in H_2O) was purchased from ALDRICH. Ammonium persulfate (APS, 98%) was purchased from Xilong Company, Guangdong, China. Nickel chloride hexahydrate ($NiCl_2$•$6H_2O$, 98%) was purchased from Sinopharm Chemical Reagent Co. Ltd, Shanghai, China. Nafion solution (5 wt%), Potassium bicarbonate ($KHCO_3$, 99%) were purchased from Alfa Aesar. All the reagents were used without further purification.

Synthesis of MPD/silica/NiCl₂ composite In a typical procedure, MPD (1.5 g) and $NiCl_2$•$6H_2O$ (322 mg) were dissolved in 17 mL 1 M HCl solution with vigorous stir for 30 min. After that, 11.2 g silica colloid solution was added to the above solution with stirring for another 10 min. Then the mixed solution was transferred to the refrigerator under 0 °C overnight. After that, 6 ml 1.0 M HCl solution containing 3.75 g APS was added dropwise to the mixed solution in an ice bath with vigorous stir. Then the mixed solution was again transferred to the refrigerator under 0 °C for another 12 h to finish the polymerization. Finally, the MPD/silica/$NiCl_2$ composite was obtained by freeze-drying under vacuum.

Synthesis of Ni-C-N The dried MPD/silica/$NiCl_2$ composite was subjected to thermal activation at a 900 °C (heating rate 5 °C/min) under Ar flow for 3 h in a tube furnace. Then the carbon-silica composite obtained after pyrolysis was treated with 1 M NaOH solution (50 vol % ethanol-50 vol % H_2O) twice at 80 °C to remove the silica template. The template-free carbon product was then leached at 80 °C in 2 M H_2SO4 for 12 h to remove metal particles and unstable species. Afterward, the sample was filtered, washed with ethanol, and dried at 60 °C to get the final Ni-C-N catalyst.

Synthesis of catalyst without Ni decoration (denoted as N-C) The catalyst without Ni decoration (N-C) was prepared in a similar way but in the absence of $NiCl_2$. Typically, 1.5 g MPD and 11.2 g silica colloid solution were added into 17 mL 1 M HCl solution. The mixed solution was stirred for 30 min and then cooled down to 0 °C. After that, 6 ml 1.0 M HCl solution containing 3.75 g APS was used to repeat the process of polymerization. After the procedures of freeze drying, calcination and etching, the N-C catalyst was obtained.

Characterization TEM images and EDX elemental mapping were performed on Tecnai G2 F20 S-TWIN with an acceleration voltage of 200 kV. HAADF-STEM images were obtained on a Cs-corrected FEI Titan G2 60-300 Microscope operated at 300 kV. Probe Cs corrector was applied to get better spatial resolution. X-ray diffraction (XRD) patterns were recorded on D/MAX-TTRIII (CBO) (Rigaku Corporation) with Cu Kα radiation (λ=1.54 Å) at a scanning rate of 5° min^{-1}. The microstructure was studied by Raman spectra using Renishaw in Via Raman microscope with 514 nm laser excitation. X-ray photoelectron spectroscopy (XPS) was conducted on a Thermo Scientific ESCALAB 250 Xi XPS system, in which the analysis chamber pressure was 1.5×10^{-9} mbar and the size of the X-ray spot was 500 um. Specific surface area was measured based on a Brunauer–Emmett–Teller (BET) method at −196 °C with a Micromeritics ASAP 2010 analyzer. The inductively coupled plasma mass spectrometry (ICP-MS) data were taken from NexION 300X (PerkinElmer). X-ray absorption spectroscopy (XAS) was collected at room temperature in transmission mode at beamline 1W1B of the Beijing Synchrotron Radiation Facility (BSRF), using a Si (111) double-crystal monochromator. Energy calibration was performed with Ni foil, and the intensity of the incident and transmitted X-rays was monitored by standard N_2-filled ion chambers. Athena and Artemis codes were used to extract the data and fit the profiles.

Electrochemical measurements Cathode catalyst inks were prepared by dispersing 5 mg sample and 10 µl Nafion solution into 0.99 ml ethanol solution. The inks were then sonicated for 1-2h to get a homogeneous solution. 50uL of the homogeneous ink was loaded onto a glassy carbon electrode with 0.5 cm diameter. 50uL of the homogeneous ink was loaded onto the carbon fiber paper with 1.0 cm×1.0 cm. The electrode was then dried at room temperature for 2 h. CO_2 electroreduction experiments were carried out in a customized airtight, two-compartment, three-electrode cell. The compartments of the cell were separated by a Nafion-115 proton exchange membrane. The carbon paper with a size of 1.0 cm×2.0 cm (catalyst painted onto the carbon fiber paper with 1.0 cm×1.0 cm) was used as the working electrode for the test at each potential. A glassy carbon electrode with 0.5 cm diameter was used as the working electrode for the test of CV. The Ag/AgCl (saturated KCl) and Pt plate (99.9%) were used as the reference electrode and counter electrode, respectively. The CO_2 electroreduction was tested in aqueous 0.5 M $KHCO_3$ at room temperature and under atmospheric pressure. The electrolyte was purged with CO_2 for at least 30 min before each controlled-potential electrolysis and the flow rate of CO_2 was maintained at 25 mL min^{-1} for all experiments. The cathodic electrolyte was stirred at a rotation rate of 1000 rpm using a magnetic stirrer. Cyclic voltammetry (CV) test was performed from −0.72 to −1.92 V *vs.* Ag/AgCl in Ar saturated 0.5 M $KHCO_3$ (pH=8.8) and −0.62 to −1.82 V *vs.* Ag/AgCl in CO_2 saturated 0.5 M $KHCO_3$ (pH=7.2) electrolyte with a scan rate of 5 mV s^{-1}. The potentials were controlled by electrochemical station (CHI760E). All potentials in this study were measured against the Ag/AgCl reference electrode and calculated with respect to the reversible hydrogen electrode (RHE) scale using E (*vs.* RHE) = E (*vs.* Ag/AgCl) + 0.1989 V + 0.059 × pH. CO_2 gas was delivered into the cathodic compartment of the cell. Then the gas phase composition vented into gas chromatograph (GC, Shimadzu GC-2014C). The gas products were analyzed by GC every 15 min. The gas concentration was averaged over three measurements. Liquid product was characterized by ^1H NMR on Bruker AVANCE III HD 400 using a pre-saturation

sequence. Liquid product concentration was quantified using dimethyl sulfoxide (DMSO) as the internal standard. The faradic efficiency and turnover frequency are calculated by the equations as follows [32]:

$$FE_{CO} = \frac{J_{CO}}{J_{total}} = \frac{v_{co} \times N \times F}{J_{total}}$$

$$TOF = \frac{I_{product}/\mathrm{NF}}{m_{cat} \times \frac{\omega}{M_{Ni}}} \times 3600$$

3. Results and discussion

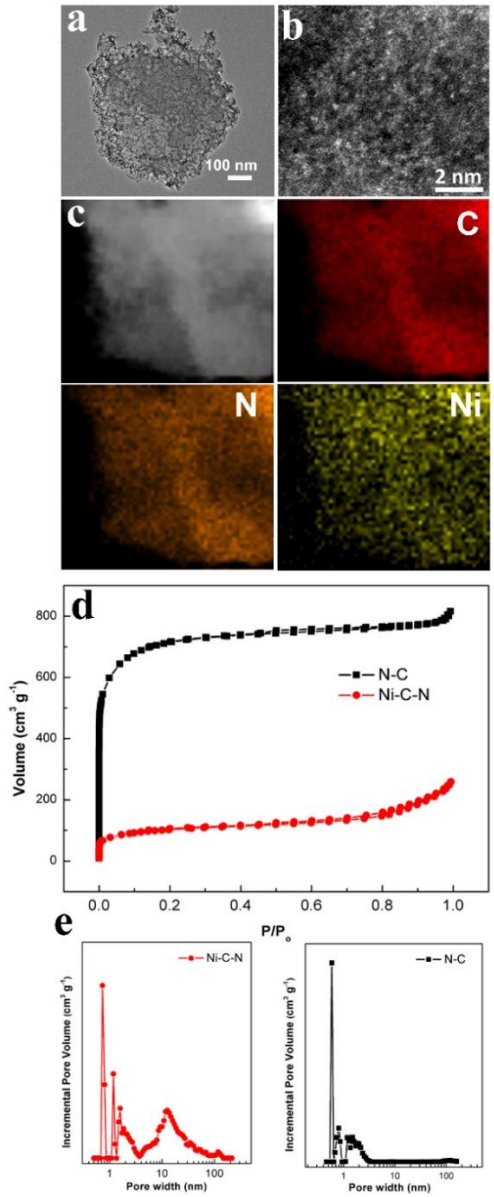

Fig. 1 (a) TEM image of Ni-C-N catalyst. (b) HAADF-STEM image of Ni-C-N catalyst. (c) EDS mapping of Ni-C-N. (d) N_2 adsorption/desorption isotherms of Ni-C-N and N-C. (e) Pore size distributions of Ni-C-N and N-C.

To synthesize Ni-C-N, the as-prepared MPD/silica/$NiCl_2$ composite was first pyrolyzed under Ar at 900 °C for 3 hours. After that the obtained solid composite were etched in NaOH to remove the templates and then etched in acid to remove metal particles and unstable species. After all these steps, the single Ni atom catalyst Ni-C-N was obtained (Fig. S1). Transmission electron microscopy (TEM) and scanning electron microscopy (SEM) showed that the as-prepared Ni-C-N catalyst exhibited a hierarchically porous structure in three scales. (Fig. 1a, Fig. S2-4). First, the catalyst possessed a three-dimensional grid structure in micrometre size (Fig. S4). The grid structure was derived from the polymer nanofibers which was formed during the process of hydrogel.[35, 36] Second, mesopores were formed because of the doping of Ni which can work as pore expanding agents in the forming of mesoporous carbon.[37] Third, the nanopores were formed because of the nanosized SiO_2 template (Fig. S4). The hierarchically porous structure helps to expose more active sites and promote more efficient mass transport in the catalytic reactions. The hierarchically porous structure was further verified by Brunauer–Emmett–Teller (BET) measurement (Fig. 1d). Although BET surface area of Ni-C-N (334.9 m^2g^{-1}) decreased compared with the sample without Ni decoration (denoted N-C) (2207.7 m^2g^{-1}), more mesopores were formed on the Ni-C-N catalyst (Fig. 1e). The decrease of BET surface area and forming of mesopores maybe caused by the Ni doping because the carbon atom around the Ni can be oxidized and gasified under high temperature.[38, 39] For a certain mass, the sample with big pore size have less surface area than that with the small one. High-angle annular dark-field scanning TEM (HAADF-STEM) images of Ni-C-N showed that the Ni species are highly dispersed as tiny clusters or single atoms while no Ni nanoparticles were observed (Fig. 1b). Energy-dispersive X-ray spectroscopy (EDS) mapping of the Ni-C-N revealed that Ni and N were homogeneously dispersed on the porous carbon (Fig. 1c). In addition, no clear peaks assignable to Ni species were observed in the XRD pattern of Ni-C-N (Fig. S5), further indicating the formation of atomically dispersed Ni on nitrogen-doped porous carbon. Raman spectra of Ni-C-N exhibited peaks at 1358 and 1596 cm^{-1}, confirming the local carbon structures contain both graphitic and disordered carbon atoms (Fig. S6). [40] The atomic ratio of Ni in Ni-C-N determined by XPS was 0.354 at% (1.65 wt%), according with the result obtained from inductively coupled plasma atomic emission spectroscopy (ICP-AES) (1.63 wt%)(Fig. S5).

The chemical configurations around Ni sites were further characterized by X-ray absorption spectroscopy (XAS). The local chemical configuration of Ni-C-N was determined by Fourier transform (FT) of Ni K-edge EXAFS oscillation (Fig. 2a). A dominant peak of Ni-N coordination was found at 1.41 Å implying that the Ni is surrounding by N.

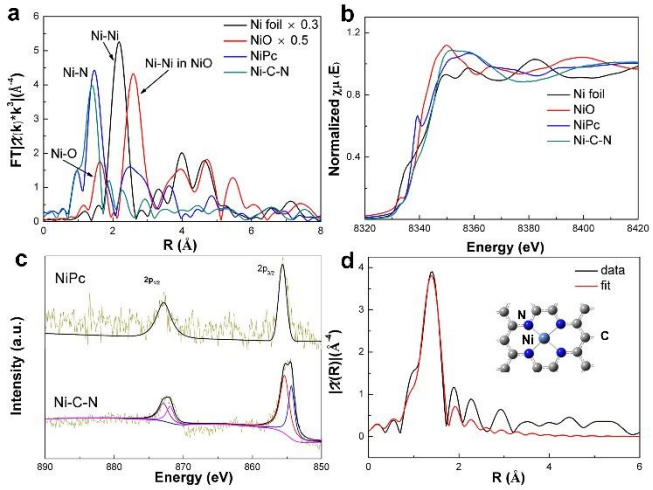

Fig. 2 (a) Fourier transformed EXAFS spectra of Ni-C-N, NiPc, NiO and Ni foil. (b) Ni K-edge XANES spectra of Ni-C-N, NiPc, NiO and Ni foil. (c) High-resolution XPS Ni 2p spectra of Ni-C-N and NiPc. (d) First-shell EXAFS fitting curve for Ni-C-N. Inset is the proposed Ni-N_4 architecture.

No obvious peak corresponding to Ni-Ni interaction were observed in Ni-C-N catalyst which further confirmed that the Ni species are dispersed as single atoms. The X-ray absorption near-edge structure (XANES) spectrum of Ni-C-N (Figure 2b) showed the intensity of the line is located between those for the Ni foil and nickel phthalocyanine (NiPc), suggesting that Ni in our catalyst is an intermediate valent state between Ni^0 and Ni^{2+}. [30, 34] This intermediate valent state can be further verified by the inflection point of the second-derivative spectra and XPS results for Ni 2p (Fig. 2c and Fig. S6). [29] In Ni-C-N, binding energies of the Ni $2p_{3/2}$ peak is dominated by the peak at 854.5 eV, which can be divided into two peaks. One is at 855.3 eV, corresponding to the Ni^{2+}, and the other is at 853.7 eV, corresponding to the metallic Ni^0. The Fourier transformed EXAFS curve of the Ni-C-N sample was fitted to give a structural model (Figure 2d). The fitting result showed Ni has been coordinated by four N atoms at a distance of ~1.85Å (Table S1).

The activities of Ni-C-N toward the CO_2 electroreduction were evaluated in a standard three-electrode H-cell with 0.5 M $KHCO_3$ aqueous solution as electrolyte. The compartments of the cell were separated by a Nafion-115 proton exchange membrane. Cyclic voltammetry (CV) were firstly used to evaluate the performances of Ni-C-N from 0 to −1.2 *vs.* RHE in Ar or CO_2 saturated 0.5 M $KHCO_3$ solutions (Fig. 3a). The onset potential of Ni-C-N was more positive in CO_2 saturated 0.5 M $KHCO_3$ solution compared with that in Ar saturated 0.5 M $KHCO_3$ solution. The cathodic current in CO_2 saturated 0.5 M $KHCO_3$ solution was also higher than that in Ar saturated 0.5 M $KHCO_3$ solution, implying the reduction of CO_2 over Ni-C-N electrode. The reduction peak in Ar saturated 0.5 M $KHCO_3$ solution implies the reduction of H_2O.

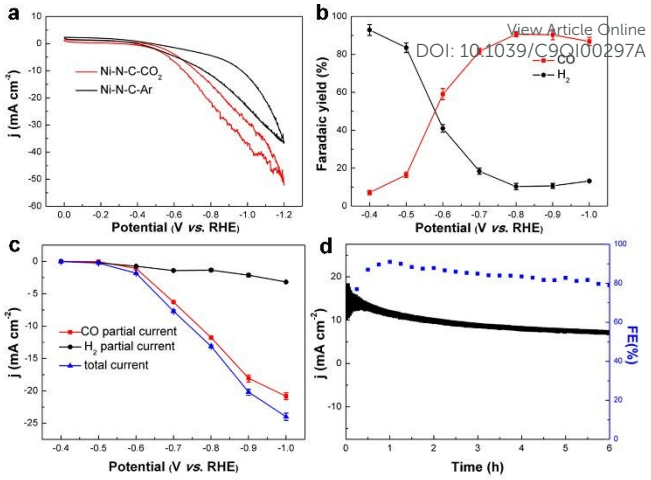

Fig. 3 (a) Cyclic voltammetry curves of Ni-C-N in Ar and CO_2 saturated 0.5 M $KHCO_3$ electrolytes, 5 mV s^{-1}. (b) FEs of H_2 and CO of Ni-C-N in CO_2 saturated 0.5 M $KHCO_3$ on applied potential. (c) Current densities of Ni-C-N catalyst on applied potential. (d) Long-term electrolysis test of Ni-C-N catalyst under −0.8 V *vs.* RHE.

The gaseous products were analyzed by gas chromatography (GC). Detectable amounts of CO and H_2 started to appear at an onset potential of −0.4 V *vs.* RHE. Then the FE of CO increased as the potential became more negative. The Ni-C-N exhibited the maximum CO FE of 90% with a current density of 11.6 mA cm^{-2} at −0.8 V *vs.* RHE. Detailed information for the dependence of CO FE on applied potential was shown in Fig. 3b. Fig. 3c showed that the CO current density increased as the potential became more negative. No liquid products were detected by ^1H NMR (Fig. S9). The stability test of Ni-C-N catalyst was performed at −0.8 V *vs.* RHE (Fig. 3d). The Ni-C-N catalyst maintained CO selectivity of 80% after 6 hours of continuous electrolysis, suggesting the good stability of the catalyst. Comparable catalytic properties of Ni-C-N were found compared with reported SACs for CO_2 electroreduction (Fig. S11 and Table S2).

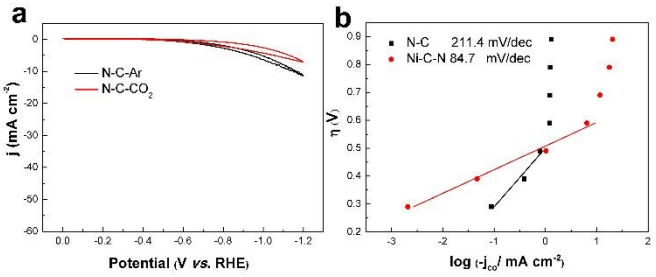

Fig. 4 (a) Cyclic voltammetry curves of N-C in Ar and CO_2 saturated 0.5 M $KHCO_3$ electrolyte, 5 mV s^{-1}. (b) Tafel plots of the partial CO current density for Ni-C-N and N-C.

To probe the active site for CO_2 reduction, the N-C catalyst without Ni doping was tested under the same condition. Although a moderate FE of CO was obtained, the current density for CO production decreased obviously for N-C catalyst (Fig. 4a and Fig. S10). Compared with the N-C catalyst, Ni-C-N showed much higher FE and current density for CO formation, which means that the single Ni sites can greatly enhance the

activity of CO_2 reduction and further prove that the single Ni atomic sites are the active sites for CO_2 reduction. [30] The Tafel slope of Ni-C-N catalyst is 84.7 mV dec^{-1}, which was much smaller than that of N-C (Fig. 4b), indicating faster kinetics of CO formation for Ni-C-N than N-C.

Conclusions

In summary, we have synthesized atomically dispersed Ni catalyst for CO_2 electroreduction via hard-templating synthesis and calcination at high-temperature. Simple operation, easy obtainment of the raw material and low cost was realized by our synthetic method. The obtained single-atom catalyst had a hierarchically porous structure and exhibited a maximum CO FE of 90% and a current density of 11.6 mA cm^{-2} at −0.8 V *vs.* RHE. A large TOF, up to 3079 h^{-1} and good durability were achieved on our catalyst. This work not only achieves synthesis of highly efficient atomically dispersed Ni catalyst for CO_2 electroreduction, but also presents a simple and low-cost method for the rational design of nanostructured catalysts at the atomic scale.

Conflicts of interest

There are no conflicts to declare

Acknowledgements

The authors acknowledge financial support from National Key Basic Research Program of China (2014CB931801 and 2016YFA0200700, Z.Y.T.), National Natural Science Foundation of China (21890381, 21721002, 21475029 Z.Y.T. and 51772957, Y.G.), Frontier Science Key Project of Chinese Academy of Sciences (QYZDJ-SSW-SLH038, Z.Y.T.), and K.C.Wong Education Foundation (Z.Y.T.).

References

1. Y. Hori, H. Wakebe, T. Tsukamoto and O. Koga, *Electrochim Acta*, 1994, **39**, 1833-1839.
2. J. J. Wu, F. G. Risalvato, F. S. Ke, P. J. Pellechia and X. D. Zhou, *J Electrochem Soc*, 2012, **159**, 353-359.
3. H. Noda, S. Ikeda, Y. Oda, K. Imai, M. Maeda and K. Ito, *B Chem Soc Jpn*, 1990, **63**, 2459-2462.
4. X. Wen, L. Chang, Y. Gao, J. Han, Z. Bai, Y. Huan, M. Li, Z. Tang and X. Yan, *Inorganic Chemistry Frontiers*, 2018, **5**, 1207-1212.
5. J.-H. Zhou, D.-W. Lan, S.-S. Yang, Y. Guo, K. Yuan, L.-X. Dai and Y.-W. Zhang, *Inorganic Chemistry Frontiers*, 2018, **5**, 1524-1532.
6. W. Qiu, R. Liang, Y. Luo, G. Cui, J. Qiu and X. Sun, *Inorganic Chemistry Frontiers*, 2018, **5**, 2238-2241.
7. B. Qiao, A. Wang, X. Yang, L. F. Allard, Z. Jiang, Y. Cui, J. Liu, J. Li and T. Zhang, *Nat Chem*, 2011, **3**, 634.
8. P. Yin, T. Yao, Y. Wu, L. Zheng, Y. Lin, W. Liu, H. Ju, J. Zhu, X. Hong, Z. Deng, G. Zhou, S. Wei and Y. Li, *Angew Chem Int Ed*, 2016, **55**, 10800-10805.
9. B. Han, G. Cheng, Y. Wang and X. Wang, *Chem Eng J*, 2019, **360**, 364-384.
10. H. Guan, J. Lin, B. Qiao, X. Yang, L. Li, S. Miao, J. Liu, A. Wang, X. Wang and T. Zhang, *Angew Chem Int Ed*, 2016, **55**, 2820-2824.
11. A. S. Varela, N. Ranjbar Sahraie, J. Steinberg, W. Ju, H.-S. Oh and P. Strasser, *Angew Chem Int Ed*, 2015, **54**, 10758-10762.
12. X.-F. Yang, A. Wang, B. Qiao, J. Li, J. Liu and T. Zhang, *Accounts Chem Res*, 2013, **46**, 1740-1748.
13. L. Zhao, Y. Zhang, L.-B. Huang, X.-Z. Liu, Q.-H. Zhang, C. He, Z.-Y. Wu, L.-J. Zhang, J. Wu, W. Yang, L. Gu, J.-S. Hu and L.-J. Wan, *Nat Commun*, 2019, **10**, 1278.
14. B. Bayatsarmadi, Y. Zheng, A. Vasileff and S.-Z. Qiao, *Small*, 2017, **13**, 1700191.
15. J. Liu, F. R. Lucci, M. Yang, S. Lee, M. D. Marcinkowski, A. J. Therrien, C. T. Williams, E. C. H. Sykes and M. Flytzani-Stephanopoulos, *J Am Chem Soc*, 2016, **138**, 6396-6399.
16. X. Guo, G. Fang, G. Li, H. Ma, H. Fan, L. Yu, C. Ma, X. Wu, D. Deng, M. Wei, D. Tan, R. Si, S. Zhang, J. Li, L. Sun, Z. Tang, X. Pan and X. Bao, *Science*, 2014, **344**, 616.
17. M.-M. Shi, D. Bao, B.-R. Wulan, Y.-H. Li, Y.-F. Zhang, J.-M. Yan and Q. Jiang, *Adv Mater*, 2017, **29**, 1606550.
18. N. Cheng, S. Stambula, D. Wang, M. N. Banis, J. Liu, A. Riese, B. Xiao, R. Li, T.-K. Sham, L.-M. Liu, G. A. Botton and X. Sun, *Nat Commun*, 2016, **7**, 13638.
19. H. J. Qiu, Y. Ito, W. Cong, Y. Tan, P. Liu, A. Hirata, T. Fujita, Z. Tang and M. Chen, *Angew Chem Int Ed*, 2015, **54**, 14031-14035.
20. Y. Chen, S. Ji, Y. Wang, J. Dong, W. Chen, Z. Li, R. Shen, L. Zheng, Z. Zhuang, D. Wang and Y. Li, *Angew Chem Int Ed*, 2017, **56**, 6937-6941.
21. A. Zitolo, V. Goellner, V. Armel, M.-T. Sougrati, T. Mineva, L. Stievano, E. Fonda and F. Jaouen, *Nat Mater*, 2015, **14**, 937.
22. T. N. Huan, N. Ranjbar, G. Rousse, M. Sougrati, A. Zitolo, V. Mougel, F. Jaouen and M. Fontecave, *ACS Catal*, 2017, **7**, 1520-1525.
23. Y. Pan, R. Lin, Y. Chen, S. Liu, W. Zhu, X. Cao, W. Chen, K. Wu, W.-C. Cheong, Y. Wang, L. Zheng, J. Luo, Y. Lin, Y. Liu, C. Liu, J. Li, Q. Lu, X. Chen, D. Wang, Q. Peng, C. Chen and Y. Li, *J Am Chem Soc*, 2018, **140**, 4218-4221.
24. Y. Cheng, S. Zhao, B. Johannessen, J.-P. Veder, M. Saunders, M. R. Rowles, M. Cheng, C. Liu, M. F. Chisholm, R. De Marco, H.-M. Cheng, S.-Z. Yang and S. P. Jiang, *Adv Mater*, 2018, **30**, 1706287.
25. Y. Jiao, Y. Zheng, P. Chen, M. Jaroniec and S.-Z. Qiao, *J Am Chem Soc*, 2017, **139**, 18093-18100.
26. F. Yang, P. Song, X. Liu, B. Mei, W. Xing, Z. Jiang, L. Gu and W. Xu, *Angew Chem Int Ed*, 2018, **57**, 12303-12307.
27. P. Su, K. Iwase, S. Nakanishi, K. Hashimoto and K. Kamiya, *Small*, 2016, **12**, 6083-6089.
28. C. Zhang, S. Yang, J. Wu, M. Liu, S. Yazdi, M. Ren, J. Sha, J. Zhong, K. Nie, A. S. Jalilov, Z. Li, H. Li, B. I. Yakobson, Q. Wu, E. Ringe, H. Xu, P. M. Ajayan and J. M. Tour, *Advanced Energy Materials*, 2018, **8**, 1703487.
29. H. B. Yang, S.-F. Hung, S. Liu, K. Yuan, S. Miao, L. Zhang, X. Huang, H.-Y. Wang, W. Cai, R. Chen, J. Gao, X. Yang, W.

View Article Online
DOI: 10.1039/C9QI00297A

Chen, Y. Huang, H. M. Chen, C. M. Li, T. Zhang and B. Liu, *Nat Energy*, 2018, **3**, 140-147.
30. K. Jiang, S. Siahrostami, T. Zheng, Y. Hu, S. Hwang, E. Stavitski, Y. Peng, J. Dynes, M. Gangisetty, D. Su, K. Attenkofer and H. Wang, *Energy Environ Sci*, 2018, **11**, 893-903.
31. K. Jiang, S. Siahrostami, A. J. Akey, Y. Li, Z. Lu, J. Lattimer, Y. Hu, C. Stokes, M. Gangishetty, G. Chen, Y. Zhou, W. Hill, W.-B. Cai, D. Bell, K. Chan, J. K. Nørskov, Y. Cui and H. Wang, *Chem*, 2017, **3**, 950-960.
32. C. Zhao, X. Dai, T. Yao, W. Chen, X. Wang, J. Wang, J. Yang, S. Wei, Y. Wu and Y. Li, *J Am Chem Soc*, 2017, **139**, 8078-8081.
33. X. Li, W. Bi, M. Chen, Y. Sun, H. Ju, W. Yan, J. Zhu, X. Wu, W. Chu, C. Wu and Y. Xie, *J Am Chem Soc*, 2017, **139**, 14889-14892.
34. C. Yan, H. Li, Y. Ye, H. Wu, F. Cai, R. Si, J. Xiao, S. Miao, S. Xie, F. Yang, Y. Li, G. Wang and X. Bao, *Energy Environ Sci*, 2018, **11**, 1204-1210.
35. D. Li, J. Huang and R. B. Kaner, *Accounts Chem Res*, 2009, **42**, 135-145.
36. L. Pan, G. Yu, D. Zhai, H. R. Lee, W. Zhao, N. Liu, H. Wang, B. C. K. Tee, Y. Shi, Y. Cui and Z. Bao, *Proceedings of the National Academy of Sciences*, 2012, **109**, 9287.
37. A. Tomita, Y. Yuhki, K. Higashiyama, T. Takarada and Y. Tamai, *Nenryo Kyokaishi (Journal of the Fuel Society of Japan)*, 1985, **64**, 402-408.
38. M. Sevilla and A. B. Fuertes, *Carbon*, 2006, **44**, 468-474.
39. H. Yasuda, H. Tamai, M. Ikeuchi and S. Kojima, *Adv Mater*, 1997, **9**, 55-58.
40. W. Zhang, Z.-Y. Wu, H.-L. Jiang and S.-H. Yu, *J Am Chem Soc*, 2014, **136**, 14385-14388.